LETTERS
PUBLISHED ONLINE: 24 APRIL 2017 | DOI: 10.1038/NNANO.2017.58
nature nanotechnology

Amyloid fibril systems reduce, stabilize and deliver bioavailable nanosized iron

Yi Shen[1†], Lidija Posavec[2†], Sreenath Bolisetty[1], Florentine M. Hilty[2], Gustav Nyström[1], Joachim Kohlbrecher[3], Monika Hilbe[4], Antonella Rossi[5,6], Jeannine Baumgartner[7], Michael B. Zimmermann[2*] and Raffaele Mezzenga[1*]

Iron-deficiency anaemia (IDA) is a major global public health problem[1]. A sustainable and cost-effective strategy to reduce IDA is iron fortification of foods[2], but the most bioavailable fortificants cause adverse organoleptic changes in foods[3,4]. Iron nanoparticles are a promising solution in food matrices[5–7], although their tendency to oxidize and rapidly aggregate in solution severely limits their use in fortification[8]. Amyloid fibrils are protein aggregates initially known for their association with neurodegenerative disorders, but recently described in the context of biological functions in living organisms[9–13] and emerging as unique biomaterial building blocks[14–16]. Here, we show an original application for these protein fibrils as efficient carriers for iron fortification. We use biodegradable amyloid fibrils from β-lactoglobulin, an inexpensive milk protein with natural reducing effects[17], as anti-oxidizing nanocarriers and colloidal stabilizers for iron nanoparticles. The resulting hybrid material forms a stable protein–iron colloidal dispersion that undergoes rapid dissolution and releases iron ions during acidic and enzymatic *in vitro* digestion. Importantly, this hybrid shows high *in vivo* iron bioavailability, equivalent to ferrous sulfate in haemoglobin-repletion and stable-isotope studies in rats, but with reduced organoleptic changes in foods. Feeding the rats with these hybrid materials did not result in abnormal iron accumulation in any organs, or changes in whole blood glutathione concentrations, inferring their primary safety. Therefore, these iron–amyloid fibril hybrids emerge as novel, highly effective delivery systems for iron in both solid and liquid matrices.

Anaemia is a major global health problem affecting 2.2 billion people worldwide[1]. Iron fortification of foods can reduce IDA, but fortification with iron is difficult because the most bioavailable water-soluble fortificants, such as ferrous sulfate and sodium iron ethylenediaminetetraacetic acid (EDTA)[3,4], tend to cause adverse sensory changes in foods. Poorly soluble fortificants, such as ferric pyrophosphate and ferrous fumarate are less reactive, but generally have lower bioavailability and/or aggregate in liquid food matrices[3]. Recently, newly developed iron nanoparticles have shown high bioavailability and low reactivity compared with ferrous sulfate and sodium iron EDTA[5–7], and have been proposed as novel iron fortificants. However, iron nanoparticles are easily oxidized and undergo rapid aggregation in solution due to their limited colloidal stability[3] limiting their use in fortification[8]. Here, we report a novel β-lactoglobulin fibrils–Fe nanoparticle hybrid material for use in iron fortification and its evaluation in both *in vitro* digestion and *in vivo* bioavailability studies. We found that the material's reducing effect, colloidal stability, improved sensory performance and high bioavailability make it promising for nutritional applications.

β-lactoglobulin (BLG) amyloid fibrils were recently used as a green reducing agent to produce gold crystals[17]. Can this reducing ability of BLG nanofibrils apply to iron and help reduce iron into its more bioavailable Fe(II) state? To answer this question, we mixed a $FeCl_3$ solution with BLG fibrils and found that the Fe(III) ions converted into Fe(II) ions. The more fibrils that were added to $FeCl_3$, the more Fe(II) ions that were detected (Fig. 1a). To investigate which amino acids (AAs) are responsible for this reducing effect, all the AAs from the primary structure of BLG (Supplementary Fig. 1a) were tested. Cysteine, tyrosine and tryptophan were all found to have a reducing effect (Supplementary Fig. 1a). However, cysteine reduced Fe(III) to Fe(II) at a much higher rate compared with tyrosine and tryptophan when prepared at their corresponding ratios as present in BLG (Supplementary Fig. 1b): the reduction rate of cysteine alone is comparable to that of the three amino acids combined, demonstrating the dominant reducing effect of cysteine. Cysteine residues in BLG contain sulfhydryl groups, which are redox active and can be easily oxidized and form disulfide bonds, normally contributing to protein tertiary structures[18–20]. During fibrillization, BLG unfolds making cysteine residues more accessible in the bulk (Supplementary Fig. 1c), thus enhancing the reducing effect. This was also demonstrated by the fact that the production of Fe(II) ions (Fig. 1b) increased when a constant amount of $FeCl_3$ was mixed with BLG fibrils with increasing fibrillization level. This trend stayed and was enhanced over 20 h (Supplementary Fig. 1d). Additionally, the reducing effect of pure fibrils and peptides was tested separately and compared with their mixture solution, which was used to develop the hybrid material, and native BLG. We found that pure fibrils and the mixture solution have a similar reducing effect, which is higher than native BLG but lower than non-fibril peptides (Supplementary Fig. 1e). This means both pure fibrils and non-fibrils contain cysteine groups, which is consistent with previous studies[21]. However, non-fibril peptides are present in very low concentration: the conversion rate of fibrils indicates 85% (±2.7%) pure fibrils. Using this number, the reducing contribution from fibrils and peptides can be obtained (Supplementary Fig. 1f).

[1]Laboratory of Food and Soft Materials, Department of Health Sciences and Technology, ETH Zurich, Schmelzbergstrasse 9, Zurich 8092, Switzerland. [2]Human Nutrition Laboratory, Department of Health Sciences and Technology, ETH Zurich, Schmelzbergstrasse 7, Zurich 8092, Switzerland. [3]Laboratory for Neutron Scattering and Imaging, PSI Paul Scherrer Institute, Villigen 5232, Switzerland. [4]Institute of Veterinary Pathology, Vetsuisse Faculty, University of Zurich, Zurich 8057, Switzerland. [5]Laboratory for Surface Science and Technology, Department of Materials, ETH Zurich, Vladimir-Prelog-Weg 5, Zurich 8093, Switzerland. [6]Dipartimento di Scienze Chimiche e Geologiche, Università degli Studi di Cagliari, INSTM Unit, Cittadella Universitaria di Monserrato, I-09100 Cagliari, Italy. [7]Centre of Excellence for Nutrition, North-West University Potchefstroom, Potchefstroom 2531, South Africa. †These authors contributed equally to this work. *e-mail: michael.zimmermann@hest.ethz.ch; raffaele.mezzenga@hest.ethz.ch

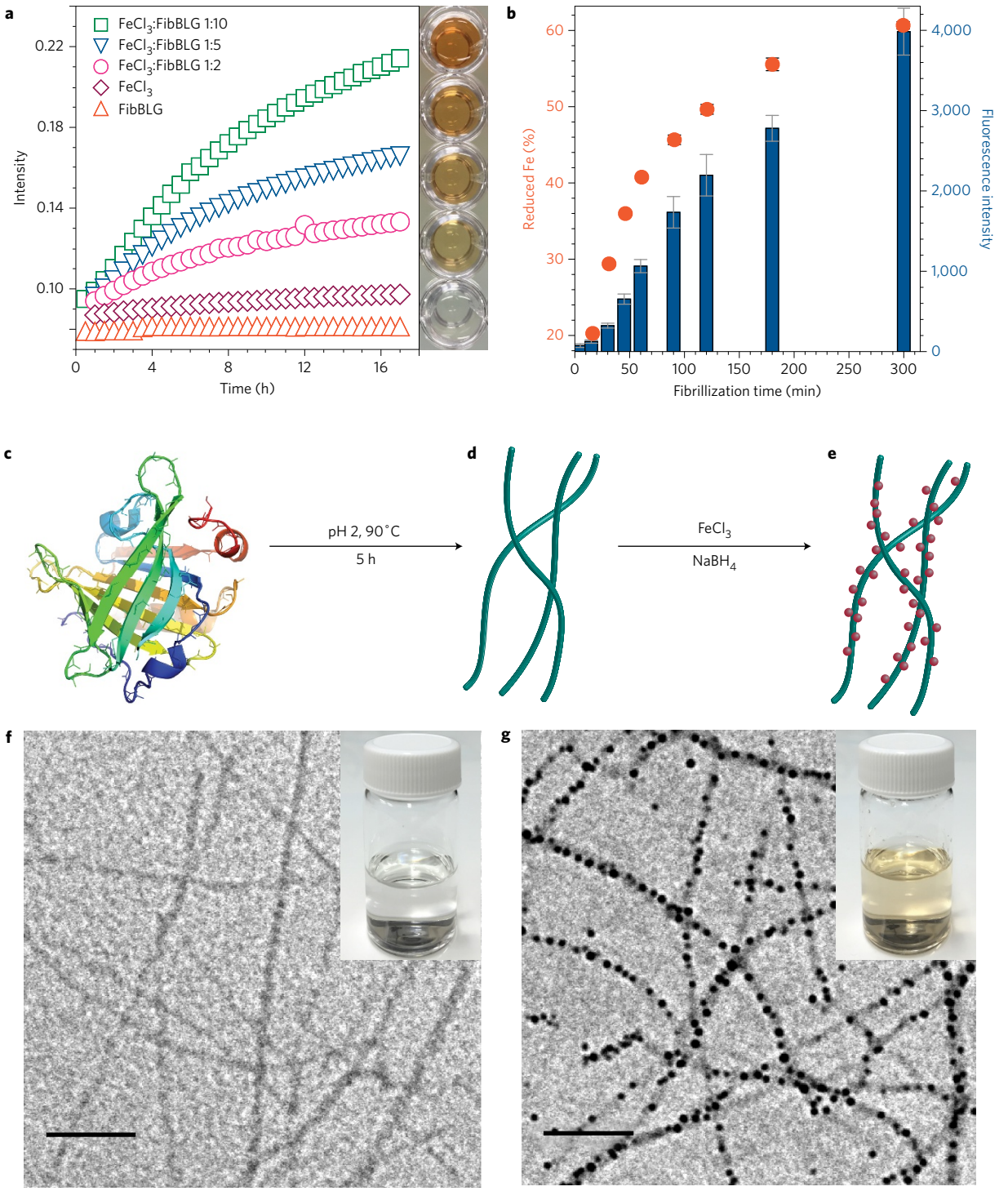

Figure 1 | Reducing effect of BLG fibrils on iron. a, Fe(II) concentration increases with time and with increasing BLG fibrils:$FeCl_3$ weight ratio, indicated by the Fe(II)-phenanthroline complex with absorbance at wavelength 512 nm, as shown in the images to the right of the plot where greater colour intensity corresponds to an increased conversion of Fe(III) to Fe(II). $FeCl_3$ and BLG fibrils were tested individually as controls. Error bars from three experiments are too small to be shown. **b**, Amount of reduced iron (red dots) increases when mixing with BLG fibrils with increasing fibrillization level at different fibrillization time points, as indicated by the fluorescence intensity of the staining agent thiazole orange (blue bars) (error bars are standard deviations from three experiments). **c**–**e**, Schematic showing BLG fibrils and the synthesis of iron–BLG fibril nanocomposites. Native β-lactoglobulin proteins (BLG) were incubated at pH 2 and 90 °C for 5 h to form amyloid fibrils (**d**). By mixing amyloids with iron chloride and sodium borohydride reducing agent, iron nanoparticles were nucleated onto the fibrils (**e**). **f**,**g**, TEM images of pure BLG fibrils (**f**) and iron–BLG fibril nanocomposites (**g**), with insets showing their respective suspensions. Scale bars, 100 nm.

Fibrils contribute mainly to the reducing effect when the unseparated fibrils solution is used. All of these results indicate that BLG fibrils are ideal candidates for iron fortification because they can maintain the iron in the more bioavailable Fe(II) state. This may also protect iron against dietary inhibitors such as phytate[22], polyphenols[23] and calcium[24].

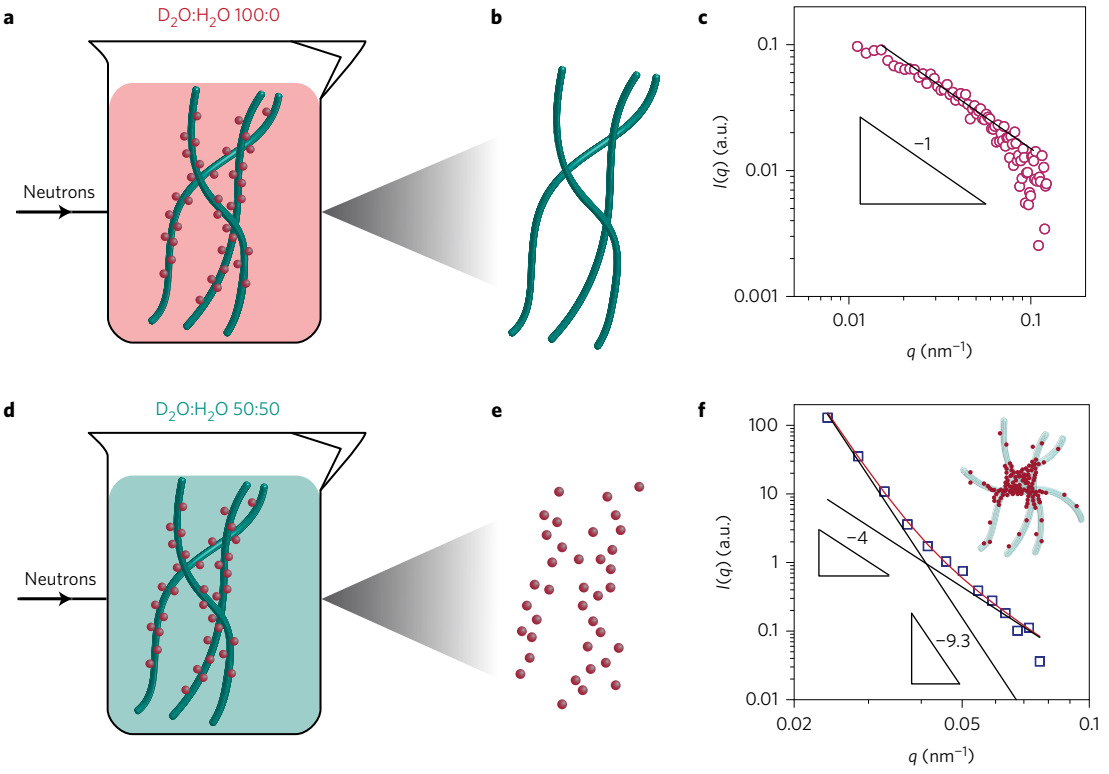

Figure 2 | Schematic illustrations and experimental results of contrast-matching small angle neutron scattering (SANS) on iron–BLG fibril hybrid suspensions. a, The D_2O:H_2O 100:0 ratio is used to contrast-match the scattering length density of the iron. **b**, Only BLG fibrils scatter and are detected. **c**, The circles represent the intensity scattered by BLG fibrils, decaying as q^{-1}, in agreement with the scattering behaviour of thin, very-long, rod-shaped objects. **d**, The D_2O:H_2O 50:50 ratio is used to contrast-match the scattering length density of iron nanoparticles. **e**, Only iron nanoparticles scatter and are detected. **f**, The squares show the signal from scattering iron nanoparticles, fitted using a sum of two potential laws. This scattering profile has its origin in larger Fe clusters that are present where several fibrils cross each other. In this region, the nanoparticles have larger size distribution, deviate from trivial spherical shape and are very densely packed, filling space with a gradient of scattering length.

Iron nanoparticles generally show good bioavailability and sensory performance but cannot be used in aqueous drinks and foods because of strong colloidal aggregation[7]. We generated iron nanoparticles *in situ* directly onto the surface of BLG fibrils (Fig. 1c–e) to provide the twofold benefits of preventing colloidal aggregation and preserving the iron in the Fe(II) state. Fe (III) ions strongly bind onto premade fibrils[25] due to their high affinity to proteins, via supramolecular coordination bonds[20,26,27]. Iron nanoparticles were thus nucleated on the surface of fibrils by adding sodium borohydride (Fig. 1e)[28]. This strong reducing agent converted iron ions into iron nanoparticles immediately after mixing although the reducing ability quickly dropped with time, leaving the BLG fibrils as sole long-term reducing agent. Similar to the pure BLG fibrils solution (Fig. 1f), the iron–BLG fibrils (Fe–FibBLG) dispersion is transparent, with a slightly darker colour, and is stable against sedimentation (Fig. 1g). In contrast, dispersions with iron nanoparticles (Fe-Nano) directly reduced without proteins were not stable, and rapidly precipitated into black iron clusters (Supplementary Fig. 2). Transmission electron microscopy (TEM) provided insight into the morphology of these hybrids before and after nanoparticle formation. Compared with the typical morphology of BLG fibrils (Fig. 1f), small (5–20 nm in diameter), spherical nanoparticles were found to decorate the surface of the fibrils (Fig. 1g). Furthermore, the Fe–FibBLG solution could be converted into a gel by the addition of NaCl and freeze-dried into powders (Supplementary Fig. 3a,b), simplifying transportation and mixing with food products. After re-dispersing the dried material, the iron nanoparticles were found to be intact, as determined by TEM analysis (Supplementary Fig. 3c). These results show that a stable iron–BLG fibril hybrid material can be produced by a simple chemical reaction and can be processed in liquid, gel or powder forms.

X-ray photoelectron spectroscopy (XPS) measurements were carried out on freshly made Fe–FibBLG and Fe-Nano powder samples to investigate the hybrid's composition. Around the core of the nanoparticles, XPS detected the presence of Fe(II) oxide for Fe-FibBLG and Fe(III) oxide for Fe-Nano. Additionally, and in all cases, Fe(III) oxi-hydroxide also formed around the cores, with the residual Fe(II)-Cl_2 and Fe(III)-Cl_3 on the surface (Supplementary Table 1). The presence of iron chlorides on the surface is due to the sample preparation; the samples being freeze-dried without washing (Supplementary Fig. 4b). The peak area ratio of Fe(0):Fe(II):Fe(III) is 0.9:74.8:24.3 for Fe–FibBLG and 29.5:33.2:37.3 for Fe-Nano (Supplementary Table 1). This indicates that the Fe–FibBLG powder contains a high concentration of Fe(II).

Contrast-matching small angle neutron scattering (SANS) was performed to measure the overall distribution of BLG fibrils and iron nanoparticles in solution (Fig. 2). We matched first the scattering length density of iron nanoparticles using 100% D_2O (Fig. 2a). Under this condition, only BLG fibrils can scatter neutrons (Fig. 2b) and the resulting scattering pattern follows the typical slope of −1 revealing the rod-like nature of the fibrils (Fig. 2c). On the other hand, when matching the scattering length density of BLG fibrils with a previously determined 50:50 D_2O:H_2O ratio (Fig. 2d and Supplementary Fig. 8), only iron particles are visible (Fig. 2e). We found a steep decay slope, which can be described by a sum of two potential laws of q^{-4} and $q^{-9.3}$, where the transition from one to the other scattering regime occurs at $q = 0.041$ nm^{-1}. q is the scattering vector, defined as $q = 4\pi \sin(\theta/2)/\lambda$, where λ is the neutron wavelength and θ is the scattering angle. The fact that we see only these large potential laws

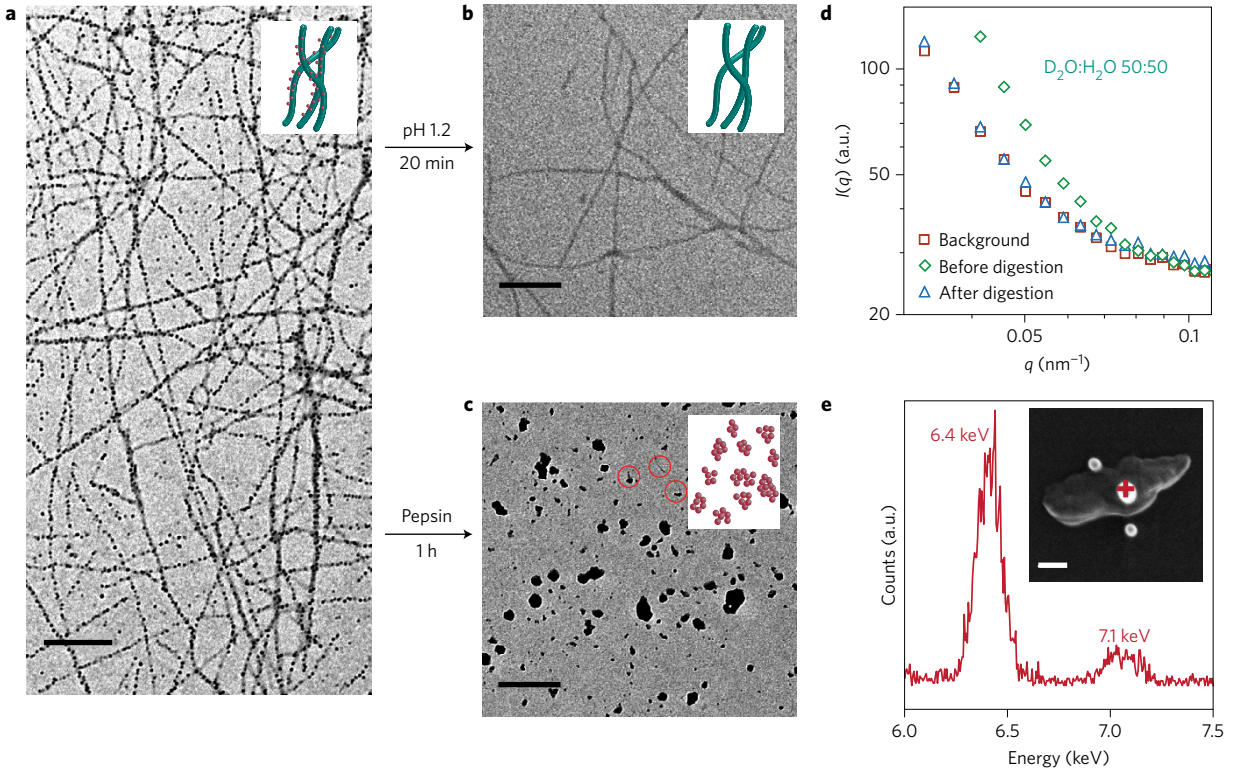

Figure 3 | *In vitro* acidic/enzymatic digestion of iron–BLG fibrils characterized by TEM, SANS and EDX. a, TEM image of BLG fibrils fully decorated with iron nanoparticles. **b**, By decreasing the pH value to 1.2 at 37 °C for 20 min, the iron particles are readily dissolved and only fibrils are detected by TEM. **c**, Fibrils are digested by pepsin at 37 °C for 1 h, resulting in the aggregation of iron nanoparticles. Red circles indicate the occasional presence of shortened, partially digested fibrils. Scale bars, 200 nm. **d**, In SANS data, D_2O:H_2O 50:50 ratio is used to contrast-match BLG fibrils. The green diamonds represent the iron–BLG fibril sample, with only iron nanoparticles detectable. After acidic digestion, all the particles are dissolved and the detected signal (blue triangles) drops and overlaps with the background scattering signal (red squares). **e**, EDX was performed on the resulting iron nanoparticle aggregates, after enzymatic digestion only, on the same sample as in **c**. The peaks at 6.4 keV and 7.11 keV are characteristic for iron. The inset shows a scanning transmission electron microscope image of the clump. Scale bar, 20 nm.

means that large iron clusters are also present. As the scattering intensity scales with the square of the volume of the clusters, only a few of them are enough to dominate the SANS signal, yielding the $q^{-9.3}$ observed dependence. The presence of a few large clusters can also be seen in TEM images, which show that such clusters are formed preferably at the cross points of several fibrils (Supplementary Fig. 9a,b). The red curve in Fig. 2f is the model fit (see Supplementary Information for details) to the experimental data including the two fitted potential scattering laws.

We then investigated the hybrid's performance during *in vitro* digestion to evaluate its potential digestibility in the upper gastrointestinal tract. First, digestion of the hybrid material with combined acidic dissolution and enzymatic hydrolysis was performed at stomach physiological conditions of both pH 1.2 and pH 2. Only a few short, thin fibrils can be found in the TEM images (Supplementary Fig. 5). To observe the dynamic digestion of iron nanoparticles and protein fibrils individually, we also performed acidic dissolution and enzymatic hydrolysis separately. We found that the iron particles were no longer observed and that only the fibrils remained after acidic dissolution (Fig. 3a,b). Additionally, SANS was performed before and after the acidic digestion, where BLG fibrils were contrast-matched to become invisible in the experiment. The results clearly show that the curve for after acidic digestion of the nanoparticles overlaps with the background curve (Fig. 3d), revealing a complete dissolution of the iron nanoparticles (Fig. 3b).

Similarly, enzymatic hydrolysis was performed on the hybrid material. BLG fibrils were hydrolysed by pepsin into short peptides[14,29] and the iron nanoparticles agglomerated with protein residues forming large clumps as shown in Fig. 3c. The composition of these aggregates was confirmed by energy dispersive X-ray spectroscopy (EDX). A clear iron signal from these aggregates was found at the peaks 6.4 and 7.1 keV (Fig. 3e). A few short BLG fibrils could still be detected (Fig. 3c, red circles) after 1-h digestion, consistent with results of the combined digestion and enzymatic hydrolysis protocol, indicating a slow enzymatic hydrolysis of fibrils compared with the fast acidic dissolution of iron nanoparticles. This difference in digestion kinetics allows the delivery of iron ions before the digestion of fibrils at low pH conditions in the stomach, hence avoiding the aggregation of iron particles, yet allowing the digestion of both the organic and inorganic phases via a synergistic acidic–enzymatic digestion.

Water-soluble $FeSO_4$ is well-absorbed in both rats and humans and, owing to its high bioavailability, is used as a reference standard[4], yet it causes adverse sensory changes in reactive food matrices. The relative bioavailability (RBV) compared with $FeSO_4$ of the nanostructured Fe–FibBLG in solid form and its potential toxicity were investigated *in vivo* (Fig. 4a) using the haemoglobin repletion bioassay in rats[30,31]. Fe-Nano synthesized without BLG fibrils was used for comparison. Animal number, diet fortification, haemoglobin (Hb) change, iron and food intake per day and body weight gain are summarized in Supplementary Table 3. Daily iron intake and Hb change over 14 days of repletion were used to plot dose-response regression lines using their respective slopes to calculate RBV (Fig. 4c). Fe–FibBLG and Fe-Nano in powder form showed RBVs of 90% and 95%, respectively, compared with $FeSO_4$ (Fig. 4d). Acidic *in vitro* digestion coupled with colorimetry was used to determine the Fe(II) percentage in Fe–FibBLG-, $FeSO_4$- and

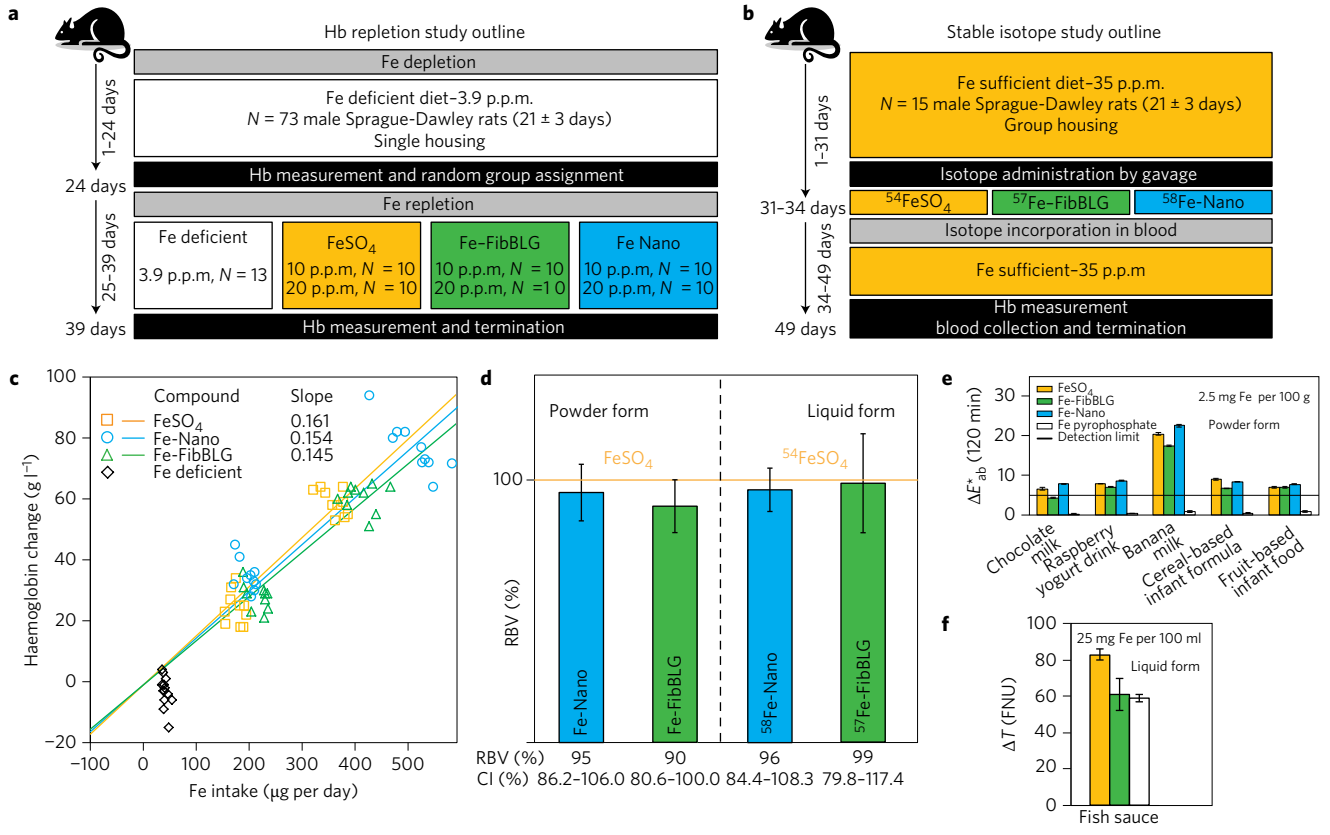

Figure 4 | Animal study design, Hb changes given by Fe–FibBLG and Fe-Nano, and colour changes after fortification. a, Outline of the Hb-repletion study. For 24–25 days, 73 rats were made iron-deficient (depletion). Over 15 days, 60 rats were fed 3 iron sources incorporated in the pellet diets with 10 or 20 p.p.m. iron (repletion). Over the entire study, 13 and 3 rats received iron-deficient (3.9 p.p.m.) and iron-sufficient (35 p.p.m.) diets, respectively. **b**, Outline of the stable isotope randomized crossover study. Stable isotopes ^{54}Fe, ^{58}Fe and ^{57}Fe were gavaged in liquid form at days 32, 33 and 34. **c**, Dose-response curves with slopes calculated for iron intake and change in Hb. **d**, RBV (%) with confidence intervals (CI) for powder and liquid compounds versus $FeSO_4$ (100%). No statistical difference in RBV was detected between compounds or when compared to $FeSO_4$ in both powder and liquid form ($p > 0.05$). **e**, Colour change of iron-containing compounds in powder form, compared with $FeSO_4$ and Fe pyrophosphate (FePP) in selected food matrices at 2.5 mg iron per 100 g food matrix. Absolute colour change, ΔE^*_{ab} ± s.d., of two replicates is given at 120 min against the non-fortified matrix. **f**, Turbidity of iron-containing compounds in liquid form, compared to $FeSO_4$ and FePP in fish source at 25 mg iron per 100 ml fish source. ΔT is relative to Formazin standard solution (FNU) and against the non-fortified fish source. Iron nano-compounds could not be tested for turbidity as they rapidly sediment in liquids (Supplementary Fig. 7).

Fe-Nano-fortified animal diets. Specifically, the diet with Fe–FibBLG contained similar amounts of Fe(II) (35 ± 4%) as $FeSO_4$ (37 ± 2%), but more than Fe-Nano (14 ± 3%). The Fe(II) data show that BLG fibrils are able to keep iron nanoparticles in the reduced form and protect them against oxidation. Extensive histological examination (Supplementary Table 5) of rat tissues after feeding and measurement of blood glutathione (GSH) was performed to assess potential toxicity. No abnormal iron accumulation or histological changes were observed, and there were no significant differences in GSH (Supplementary Table 4). Although these initial results suggest a lack of toxicity, specifically designed long-term toxicity studies are needed to confirm these findings.

The bioavailability of the compounds in liquid form was then evaluated in a stable iron isotope study (Fig. 4b). Erythrocyte incorporation of stable iron isotopes 14 days after gavage administration of ^{57}Fe–FibBLG (RBV 99%) and ^{58}Fe-Nano (RBV 96%) was not significantly different from $^{54}FeSO_4$ (Fig. 4e). The percentage of Fe(II) against total iron of Fe-Nano (84.9 ± 0.2%) and Fe–FibBLG (83.1 ± 0.4%) after acidic digestion was comparable to $FeSO_4$ (92.2 ± 0.3%) (Supplementary Table 2), possibly explaining the high RBV of Fe-Nano and Fe-FibBLG, and there was no significant difference in RBVs when comparing Fe-Nano and Fe–FibBLG. However, when added to liquids (pH 7), Fe-Nano forms a dark-yellow, turbid solution with flocculated agglomerates that tend to precipitate (Supplementary Fig. 6), whereas Fe–FibBLG forms a stable transparent dispersion, similar to the freshly made dispersion at pH 3.

Sensory performance of the hybrid in both powder and liquid forms was further analysed by their colour change and turbidity in food matrices that could be vehicles for iron fortification. $FeSO_4$ and iron pyrophosphate (FePP) were used as positive and negative standards, respectively. Selected polyphenol-rich food matrices were fortified with iron compounds in solid form at a concentration of 2.5 mg iron per 100 g and the colour change, ΔE, was determined (Fig. 4e; fortification level of 5 mg iron per 100 g is shown in Supplementary Fig. 7). FePP showed the least colour change because of its low water solubility and tendency to precipitate, but its bioavailability is generally low (Supplementary Fig. 6). $FeSO_4$, Fe–FibBLG and Fe-Nano caused colour changes due to reaction with polyphenols[7,32], however, Fe–FibBLG showed significantly less colour changes than $FeSO_4$ in most of the matrices, and for chocolate milk this change was below the detection limit of $5\Delta E^*_{ab}$, where ΔE^*_{ab} is the absolute colour change. Additionally, we evaluated the increase in turbidity after fortifying fish sauce with 25 mg iron per 100 ml and a storage time of 1 month at ambient conditions. The results show that Fe–FibBLG causes

significant lower turbidity than $FeSO_4$ (Fig. 4f). These results taken together demonstrate that Fe–FibBLG is a promising carrier and delivery system for nanosized iron, with bioavailability comparable to $FeSO_4$, but with improved sensory performance, and is colloidally more stable than standard forms of nanosized iron.

To summarize, we have combined organic and inorganic materials at the nanoscale to produce highly bioavailable and cost-effective iron–amyloid fibril hybrids. This is the first demonstration that BLG fibrils with reducing properties can be effective carriers for iron nanoparticles for food fortification. The resulting hybrid material, available in both powder and liquid forms, was shown to have excellent physical stability and chemical properties and to undergo fast acidic dissolution and enzymatic digestion, as demonstrated *in vitro*. This material has a bioavailability equivalent to $FeSO_4$ in Hb-repletion and stable-isotope studies in rats, but with less organoleptic changes in foods, and without any tissue accumulation. Additionally, its total iron content of $7.0 \pm 0.9\%$ in the powder form (corresponding to ~23.9% weight of BLG), is comparable with currently available iron fortificants[3]. The reducing-antioxidant effects, stability in aqueous dispersions, improved sensory performance and high bioavailability combined with its low cost demonstrate that iron–amyloid fibril hybrids are promising novel iron fortificants in both solid and liquid foods.

Methods

Methods and any associated references are available in the online version of the paper.

Received 16 August 2016; accepted 9 March 2017; published online 24 April 2017

References

1. Kassebaum, N. J. *et al.* A systematic analysis of global anemia burden from 1990 to 2010. *Blood* **123,** 615–624 (2013).
2. Zimmermann, M. B. & Hurrell, R. F. Nutritional iron deficiency. *Lancet* **370,** 511–520 (2007).
3. Allen, L., de Benoist, B., Dary, O. & Hurrell, R. *Guidelines on Food Fortification with Micronutrients* (World Health Organization, 2006).
4. Hurrell, R. F. Forging effective strategies to combat iron deficiency fortification: overcoming technical and practical barriers. *Heal. Promot.* **1,** 806–812 (2002).
5. Acosta, E. Bioavailability of nanoparticles in nutrient and nutraceutical delivery. *Curr. Opin. Colloid Interface Sci.* **14,** 3–15 (2009).
6. Rohner, F. *et al.* Synthesis, characterization, and bioavailability in rats of ferric phosphate nanoparticles. *J. Nutr.* **137,** 614–619 (2007).
7. Hilty, F. M. *et al.* Iron from nanocompounds containing iron and zinc is highly bioavailable in rats without tissue accumulation. *Nat. Nanotech.* **5,** 374–380 (2010).
8. Huber, D. L. Synthesis, properties, and applications of iron nanoparticles. *Small* **1,** 482–501 (2005).
9. Barnhart, M. M. & Chapman, M. R. Curli biogenesis and function. *Annu. Rev. Microbiol.* **60,** 131–147 (2006).
10. Iconomidou, V. A., Vriend, G. & Hamodrakas, S. J. Amyloids protect the silkmoth oocyte and embryo. *FEBS Lett.* **479,** 141–145 (2000).
11. Maddelein, M.-L., Dos Reis, S., Duvezin-Caubet, S., Coulary-Salin, B. & Saupe, S. J. Amyloid aggregates of the HET-s prion protein are infectious. *Proc. Natl Acad. Sci. USA* **99,** 7402–7407 (2002).
12. Fowler, D. M. *et al.* Functional amyloid formation within mammalian tissue. *PLoS Biol.* **4,** 0100–0107 (2006).
13. Maji, S. K. *et al.* Functional amyloids as natural storage of peptide hormones in pituitary secretory granules. *Science* **325,** 328–332 (2009).
14. Li, C., Adamcik, J. & Mezzenga, R. Biodegradable nanocomposites of amyloid fibrils and graphene with shape-memory and enzyme-sensing properties. *Nat. Nanotech.* **7,** 421–427 (2012).
15. Bolisetty, S. & Mezzenga, R. Amyloid–carbon hybrid membranes for universal water purification. *Nat. Nanotech.* **11,** 365–371 (2016).
16. Knowles, T. P. J. & Mezzenga, R. Amyloid fibrils as building blocks for natural and artificial functional materials. *Adv. Mater.* **28,** 6546–6561 (2016).
17. Bolisetty, S. *et al.* Amyloid-mediated synthesis of giant, fluorescent, gold single crystals and their hybrid sandwiched composites driven by liquid crystalline interactions. *J. Colloid Interface Sci.* **361,** 90–96 (2011).
18. Michaels, L. & Guzman Barron, E. S. Cysteine complexes with metals. *J. Biochem.* **83,** 191–210 (1929).
19. Brosnan, J. & Brosnan, M. The sulfur-containing amino acids: an overview. *J. Nutr.* **136,** 16365–16405 (2006).
20. Giles, N. M. *et al.* Metal and redox modulation of cysteine protein function. *Chem. Biol.* **10,** 677–693 (2003).
21. Akkermans, C. *et al.* Peptides are building blocks of heat-induced fibrillar protein aggregates of β-lactoglobulin formed at pH 2. *Biomacromolecules* **9,** 1474–1479 (2008).
22. Hallberg, L., Brune, M. & Rossander, L. Iron absorption in man: ascorbic acid and dose-dependent inhibition by phytate. *Am. J. Clin. Nutr.* **49,** 140–144 (1989).
23. Hurrell, R. F., Reddy, M. & Cook, J. D. Inhibition of non-haem iron absorption in man by polyphenolic-containing beverages. *Br. J. Nutr.* **81,** 289–295 (1999).
24. Hallberg, L., Brune, M., Erlandsson, M., Sandberg, A.-S. & Rossander-Hulten, L. Calcium: effect of different amounts on nonheme- and heme-iron absorption in humans. *Am. J. Clin. Nutr.* **53,** 112–119 (1991).
25. Adamcik, J. *et al.* Understanding amyloid aggregation by statistical analysis of atomic force microscopy images. *Nat. Nanotech.* **5,** 423–428 (2010).
26. Leal, S. S., Botelho, H. M. & Gomes, C. M. Metal ions as modulators of protein conformation and misfolding in neurodegeneration. *Coord. Chem. Rev.* **256,** 2253–2270 (2012).
27. Zhou, J. *et al.* Preparation and characterization of β-lactoglobulin hydrolysate-iron complexes. *J. Dairy Sci.* **95,** 4230–4236 (2012).
28. Sun, Y.-P., Li, X., Cao, J., Zhang, W. & Wang, H. P. Characterization of zero-valent iron nanoparticles. *Adv. Colloid Interface Sci.* **120,** 47–56 (2006).
29. Bateman, L., Ye, A. & Singh, H. *In vitro* digestion of β-lactoglobulin fibrils formed by heat treatment at low pH. *J. Agric. Food Chem.* **58,** 9800–9808 (2010).
30. Cunniff, P. & AOAC. in *Official Methods of Analysis of AOAC International* 62–63 (AOAC International, 1997).
31. Forbes, A. L. *et al.* Comparison of in vitro, animal, and clinical determinations of iron bioavailability: International Nutritional Anemia Consultative Group Task Force report on iron bioavailability. *Am. jounal Clin. Nutr.* **49,** 225–238 (1989).
32. Hurrell, R. Linking the bioavailability of iron compounds to the efficacy of iron-fortified foods. *Int. J. Vitam. Nutr. Res.* **77,** 166–173 (2007).

Acknowledgements

The authors would like to thank C. Cercamondi and C. Speich for their help in the sensory studies; A. Sánchez-Ferrer (ETHZ) for discussions on the reducing effect, F. Gramm (ETHZ) for EDX detection and STEM imaging, and the support from the ETHZ Microscopy Center (ScopeM). Authors gratefully thank for their support during the animal study: E. Kemp, H. Bunnting, C. Zeder and A. Fick. We acknowledge help from C. Zeder, A. Krzystek and T. Christ for the isotope analyses. We furthermore thank L. Molinari for performing the statistical analyses and J. Lam for the assistance in the sensory experiments. N. Spencer is gratefully acknowledged for the use of the XPS spectrometer and Mr. Cossu is thanked for the technical assistance. This work was supported by the Swiss National Science Foundation, National Research Program 69, grant number 406940-144166-1.

Author contributions

R.M. conceived the study. Y.S. and L.P. performed the experiments. Y.S., L.P., S.B., F.M.H., J.B., M.B.Z. and R.M. designed the experiments. Y.S. produced the materials. Y.S. performed reducing effect and *in vitro* digestion experiments. Y.S. and G.N. imaged the material under TEM. Y.S., S.B. and J.K. performed neutron scattering experiments and analysed the data. Y.S. and A.R. performed XPS experiments and analysed the data. L.P. and Y.S. performed animal studies, data analysis and sensory performance experiments. M.H. performed histology assessments. Y.S., L.P., R.M. and M.B.Z. co-wrote the paper.

Additional information

Supplementary information is available in the online version of the paper. Reprints and permissions information is available online at www.nature.com/reprints. Publisher's note: Springer Nature remains neutral with regard to jurisdictional claims in published maps and institutional affiliations. Correspondence and requests for materials should be addressed to M.B.Z. and R.M.

Competing financial interests

R.M., M.B.Z., Y.S. and S.B. declare to be the inventors of a patent filed by ETH Zurich related to the work presented here (EP17160624.7).

Methods

Production of hybrids. β-Lactoglobulin (BLG) was purchased from Davisco Foods International Inc. (>98%). BLG was used after dialysis and BLG amyloid fibrils were prepared based on a previously reported protocol[33]. Purified H_2O was used with varied pH values adjusted by HCl. For neutron scattering measurements, D_2O and DCl were used instead.

Iron nanoparticles were composited on BLG fibrils (Fe–FibBLG) by *in situ* chemical reduction of $FeCl_3{\cdot}6H_2O$ (97%, Sigma-Aldrich). First, 2 wt% of BLG fibrils at pH 2 were mixed with 0.1 M $FeCl_3{\cdot}6H_2O$ solution. Fe(III) ions that bound to BLG fibrils were then chemically reduced by $NaBH_4$ (≥99%, Sigma-Aldrich)[34,35]. The final concentrations of BLG fibrils, $FeCl_3$ and $NaBH_4$ were 0.45 wt%, 0.015 M and 0.026 M. The iron:protein weight ratio was 1:5. Iron nanoparticles (Fe-Nano) were obtained by reducing the $FeCl_3{\cdot}6H_2O$ solution alone with $NaBH_4$ at the same concentrations.

Reducing effect measurements

Influence of the amount of BLG fibrils. A 2 wt% BLG fibrils solution was mixed with 0.1 M $FeCl_3{\cdot}6H_2O$ (97%, Sigma-Aldrich) to reach final iron:protein weight ratios of 1:2, 1:5 and 1:10 (molecular ratios of 1:0.006, 1:0.015 and 1:0.03). The fibril solution was not separated from the unreacted peptides but obtained directly from the hydrolysed monomers as a mixture of pure fibrils and unreacted peptides, thus the molecular concentration should be read as monomer equivalent. The presence of Fe (II) ions was revealed by adding 5 mM 1,10-phenanthroline (≥99%, Sigma-Aldrich) to the solution and the distinctive orange colour was measured at 512 nm wavelength (Tecan, 200 PRO multimode reader)[6].

Test of amino acids. To measure the contribution of each amino acid (AA) residue of BLG to the reducing effect, all the AAs from the primary structure of BLG were investigated. In short, asparagine (N), cysteine (C), aspartic acid (D), glutamic acid (E), glutamine (Q), glycine (G), histidine (H), lysine (K), serine (S), arginine (R), proline (P), threonine (T), tryptophan (W), tyrosine (Y), methionine (M), leucine (L), alanine (A), isoleucine (I), phenylalanine (F) and valine (V), 20 AAs, were mixed with $FeCl_3$ to a final iron:AA weight ratio of 1:2 and measured for absorbance as described above. The AAs that did not dissolve in water were first mixed with $FeCl_3$ to react and then centrifuged, after which the supernatant was taken for the colorimetric test.

Cysteine, tryptophan, tyrosine and their mixtures were mixed with $FeCl_3$ at molecular ratios of Fe:C 5:5, Fe:W 5:2, Fe:Y 5:4 and Fe:(C + W + Y) 5:(5 + 2 + 4), which are their corresponding ratios as present in BLG. The per cent of reduced Fe(III) was then measured with time.

Accessibility of free cysteine groups. The accessibility of free cysteine groups, which contain free thiol groups, was tested and compared for the BLG fibrils system and native BLG over time. We used the protocol described previously to indicate the free thiol groups in BLG solutions by using 5,5′-dithiobis(2-nitribenzoic acid) (DTNB, ≥98%, Sigma-Aldrich)[36]. Both BLG fibrils and native BLG solutions were adjusted to pH 7 and used at a concentration of 0.05 wt%. The free thiol groups were revealed by reacting with DTNB and showing a distinct yellow colour with specific absorbance at wavelength 412 nm (Tecan, 200 PRO multimode reader).

Influence of fibrillization. The influence of the fibrillization level of BLG on the reducing effect was tested by preparing the BLG amyloid fibrils and measuring the reducing effect at selected time points. A BLG solution (2 wt%, pH 2) was incubated at 90 °C for 5 h and samples were taken after 0, 5, 15, 30, 45, 60, 90, 120, 180 and 300 min. The fluorescent dye thiazole orange was used to indicate the fibrillization level with excitation wavelength 421 nm and emission wavelength 455 nm using a plate reader (Tecan, 200 PRO multimode reader)[37]. These solutions were mixed with $FeCl_3$ with final molecular concentrations of BLG fibrils of 36.7 μM (monomer equivalent) and of $FeCl_3$ of 166.7 μM (36.7 > 166.7/5), aiming to complete the reducing reaction. Indeed, 1 M cysteine reduces 1 M $FeCl_3$. We assume all five cysteine residues in BLG are active so that for a 1 M BLG solution, theoretically a 5 M $FeCl_3$ solution is needed to complete the reaction. The amount of Fe(II) produced over time was estimated from the calibration curve made from $FeSO_4{\cdot}7H_2O$ (≥99%, Sigma-Aldrich) solutions with concentrations 0, 20, 50, 100, 200 and 400 μM. To exclude the time effect, a series of calibration curves were used at different time points. Cysteine was tested in the same experiment as a comparison.

The fibrils solution was further separated to pure fibrils and non-fibril peptides by centrifugation using a filter (MWCO 30 kDa, Amicon Ultra 15, Merck Millipore; 10 min, 10,000*g*, 20 °C). A MWCO 30 kDa filter was chosen because after fibrillization, the non-fibril peptides are all below 20 kDa (ref. 38). We also found short fibrils in the supernatant after centrifugation using a MWCO 100 kDa filter using TEM, but not 30 kDa. The conversion rate of fibrils was calculated by measuring the protein concentration of retentate (pure fibrils) and supernatant (non-fibrils peptides) using a UV–vis spectrophotometer (Cary 100, Agilent Technologies) at a wavelength of 280 nm after centrifugation. The reducing effect of both pure fibrils and peptides was measured and compared with that of fibrils mixture and native BLG at a Fe:protein weight ratio 1:5, using the colorimetric test described above.

Characterizing hybrids

Transmission electron microscopy (TEM) and energy-dispersive X-ray spectroscopy (EDX). TEM imaging was performed on copper grids covered with a carbon layer (Electron Microscopy Sciences) without staining. A 4 μl dispersion was placed on the grids for 1 min, then drained and washed with purified water twice. The images were taken on dried grids by bright-field TEM (FEI, Morgagni 268) operated at high voltage, 100 kV. A scanning-TEM (Hitachi HD 2700) was used to image the samples and detect the elements in the samples, with the same preparation procedure as for TEM.

Small angle neutron scattering (SANS). SANS experiments were performed at the SANS I beamline of the Swiss Neutron source at the Paul Scherer Institute (PSI), Switzerland. For these experiments, the samples were prepared in a series of D_2O and H_2O mixtures to obtain different scattering contrasts. The ratio 100:0 of D_2O:H_2O was chosen to contrast-match iron nanoparticles based on previous studies[39,40]. The solvent composition matching the contrast of BLG fibrils was determined by measuring BLG fibrils samples alone under SANS with D_2O:H_2O ratios of 100:0, 60:40 and 50:50 as solvents. The wavelength of the incident beam was $\lambda = 0.5269$ nm, and the sample-to-detector distance was 18 m. The q range over which the data could be reliably collected was 0.01–0.1 nm^{-1}. The raw spectra were corrected for background from the solvents, electronic noise and detector efficiency according to standard SANS I procedure. The isotropic 2D scattering spectra were radially averaged by the GRASP program. The resulting radial averaged files were further analysed using the software package SASfit[41]. Further information and discussion can be found in the Supplementary Information.

In vitro *digestion.* Combined digestion of acidic dissolution and enzymatic hydrolysis was performed at pH 1.2 and pH 2. 150 mM NaCl and 2 mg ml^{-1} pepsin were added to the solution and the samples were shaken at 50 r.p.m. and 37 °C for 1 h in a shaking water bath (GFL 1086) to simulate the physiological condition of the stomach[29]. To observe the digestion of iron nanoparticles and protein fibrils separately, *in vitro* experiments were performed at two complementary conditions. For the acidic dissolution of iron nanoparticles, 1 ml Fe–FibBLG solution with 0.08 wt% iron content was adjusted to pH 1.2 and shaken at 50 r.p.m. and 37 °C for 20 min. For the enzymatic hydrolysis of BLG fibrils, 150 mM NaCl and 2 mg ml^{-1} pepsin (from porcine gastric mucosa with 3,200–4,500 units per mg protein, Sigma-Aldrich) were added to the Fe–FibBLG solution at pH 2.7. The samples were shaken at 50 r.p.m. and 37 °C for 1 h.

In vivo *studies.* All experimental procedures were approved by the AnimCare Ethics Committee of the Faculty of Health Science of the North-West University Potchefstroom under ethics number NWU-00152-15-A5.

Depletion–repletion study

Animals and diets. The bioavailability of the Fe compounds in powder form was determined by the hemoglobin (Hb) repletion method[30,31] using two levels of 10 and 20 mg Fe per kg (p.p.m.) for each Fe source ($FeSO_4$ (dried ferrous sulfate, micronized, P. Lohmann GmbH) Fe–FibBLG and Fe-Nano). The base diet was an Fe-deficient AIN-93G (ref. 42) purified rodent diet (Dyets, Inc., Nr. 115072). Before pelleting, the different Fe sources were added to reach final fortification levels of 10, 20 or 35 ($FeSO_4$ only) p.p.m. Diet compositions are shown in Supplementary Table 6 (Extended Data). The final Fe content of all diets was verified by atomic absorption spectroscopy (AAS) (SpecrAA-240Z with GTA-120 Graphite Tube Atomizer, Varian Techtron). Male Sprague-Dawley rats ($n = 76$) were bred in the Vivarium of the North West University Potchefstroom (South Africa). At 21 ± 3 days of age, the animals were housed individually in grid (stainless steel) floor cages (Tecniplast), having *ad libitum* access to demineralized (18 MΩ, Millipore) water and diet throughout the whole study. A 12–12 h light–dark cycle (lights off at 18:00 h), room temperature of 22 ± 1 °C and relative humidity of 55 ± 15% were ensured. Body weight measurement, health check and animal handling to reduce stress at blood collection and euthanasia were performed three times per week. The animals were trained to enter the restrainer three days before sampling. The animals were depleted in Hb for a period of 24 days during which they were fed the Fe-deficient diet (3.9 p.p.m.). At the end of the depletion period, the animals were weighed, restrained and blood was collected from the tail vein into EDTA-coated capillary tubes (Microvette 200/300, Sarstedt) for the measurement of Hb (BC-5300 Vet, Auto Hematology Analyzer, Mindray). The rats were assigned to groups so that the average baseline Hb was not significantly different between groups. During the repletion period of 14 days, the rats received either one of the test compounds (10 or 20 p.p.m., $n = 10$) or the Fe-deficient diet ($n = 13$). One additional Fe-sufficient group ($n = 3$) was fed the diet containing 35 p.p.m. $FeSO_4$ and served as a control with normal organ structure for the histological investigation. At the end for the repletion period, the animals were restrained and blood was collected from the tail vein and Hb measured. Individual food intake during the repletion period was recorded every second day by subtracting the amount of food refused and spilled on the collection tray (paper lined underneath the wired cage floor) from the amount that was offered.

At the end of the study, the animals were deeply anesthetized with an intraperitoneal injection of sodium pentobarbitone (Euthapent(r), Kyron Laboratories Ltd) and blood was collected (DB Vacutainers, K_2E(EDTA)) from the beating heart.

Two aliquots were transferred to a 2 ml Eppendorf tube and stored at −80 °C for measurement of glutathione in whole blood (GSH whole blood:protein ratio).

The detailed statistical analysis of the data can be found in the Supplementary Information.

Glutathione (GSH) measurement. Briefly, whole blood was unfrozen for 1 h on ice and diluted (5% v/v) with extraction buffer. The suspension was sonicated in a cup horn sonicator (with 40% amplitude, 15 cycles of 10 s on/5 s off, 2 min and 30 s; Vibra-cell, Sonics and Materials) and centrifuged (14,000*g*, 14 min, +4 °C; Centrifuge 5418R, Eppendorf). The supernatant was collected and diluted (0.6% v/v) with extraction buffer, incubated on ice for 30 min and centrifuged (14,000*g*, 15 min, +4 °C). The second supernatant was collected and GSH was measured in duplicate using the assay described in ref. 43. The extraction buffer used in the GSH assay was prepared daily by diluting 0.1% triton-X 100 (Roche) and 0.6% sulfosalicylic acid (EDTA free, Roche) in 0.1 M potassium phosphate buffer with 5 mM EDTA disodium salt (Sigma), pH 7.5. Protein content of the second supernatant was measured in duplicate using the Pierce BCA Protein Assay Kit (Thermo Fisher Scientific) following the kit's manual for the microplate procedure. GSH and protein contents were measured at 412 nm and 562 nm wavelengths, respectively, at 20 °C (Infinite 200 Pro microplate reader, Tecan), and the final values for GSH (μM) and protein ($g\,l^{-1}$) extrapolated from a standard calibration curve and the GSH whole blood:protein ratio (μmol per gram protein) calculated.

Histology. The following organs were excised and fixed in 10% formalin for histological analysis: brain, heart, liver median lobe, stomach, duodenum, ileum, jejunum, caecum, colon, spleen, kidneys, heart, lungs and thymus. Formalin solution was prepared by mixing 1:10 v/v PBS (sodium chloride for analysis, Merck; di-sodium hydrogen phosphate dodecahydrate, for analysis, Merck; sodium di-hydrogen phosphate monohydrate, for analysis, Merck) and formaldehyde solution (formaldehyde solution 38% v/v, Medicolab cc., Amalgam). For light microscopy, tissues were dehydrated with xylene and a descending alcohol row (Tissue Tek VIP), paraffin embedded, and stained with haematoxylin & eosin (H&E), Prussian Blue for detection of Fe(III) ions and Turnbull Blue for detection of Fe(II) ions. The veterinary pathologist (University of Zurich, Switzerland) examined histologically 5–6 animals of each test group, 8 animals from the Fe-deficient group and 3 animals for the Fe-sufficient group and was unaware of the group assignment.

Stable isotopes study

Animals and diets. Male Sprague-Dawley rats ($n = 30$) were bred in the Vivarium of the North-West University Potchefstroom (South Africa). At 21 ± 3 days of age, the animals were housed in groups of three in individually ventilated cages for 31 days, having *ad libitum* access to demineralized (18 MΩ, Millipore) water and diet (35 p.p.m.) throughout the whole study with a 12–12 h light–dark cycle (lights off at 18:00 h), room temperature of 22 ± 1 °C and relative humidity of 55 ± 15%. After 31 days of adaptation, the animals were fasted for 10–12 h to ensure gastric emptiness and the food was given back daily 2 h post administration. The animals were divided into two groups ($n = 15$ each) and the isotope-labelled compound in liquid form (0.5 ml total volume) was carefully administered by gavage (stainless steel needles, G16) over three consecutive days. The administration was done in a randomized way such that each animal received the same compound ($^{54}FeSO_4$, ^{57}Fe–FibBLG and ^{58}Fe-nano) only once. For each administration, extra care was taken to ensure that the compound would reach the animal's stomach. For $^{54}FeSO_4$ and ^{57}Fe-FibBLG, the exact amount administered to the animal was calculated by subtracting the empty syringe and gavage needle weight from the full one. To record the administered amount of ^{58}Fe-Nano in the most precise way, the syringe and the gavage needle were rinsed with deionized water and the rinsing collected, water was evaporated (80 °C, 24 h), dissolved in 2 ml HNO_3 65% acid (sub boiled, Human Nutrition Laboratory, Switzerland) and measured for Fe concentration by AAS (SpecrAA-240Z with flame Atomizer, Varian Techtron). The 0.5 ml gavage dose contained 200 μg ^{54}Fe, ^{57}Fe or ^{58}Fe, therefore, below the acute toxicity level where $LD_{50}(FeSO_4) = 51$ mg Fe (ref. 44) and bigger than the detection limit of 16 μg for ICP-MS measurements[45–47]. The stable isotope method is commonly used in human studies[48] and here it was specifically applied to directly measure the fractional incorporation of iron from the compounds in liquid form using each subject as its own control.

After isotope incorporation over 15 days[49], all animals were anesthetized and the blood was collected as described in depletion–repletion study. Three aliquots were stored at −20 °C until Fe was extracted from the erythrocytes by microwave-assisted acid digestion in whole blood and analysed by ICP-MS[50]. One aliquot was stored at −80 °C and measured for GSH/protein concentration.

Isotope preparation. Stable iron isotopes (^{54}Fe, ^{57}Fe and ^{58}Fe, with isotopic enrichments of, respectively, 99.9%, 96.3% and 99.9%) were purchased from Chemgas, as elemental metal powders (>99.9% Fe). The stable isotopes ^{57}Fe–FibBLG and ^{58}Fe-Nano were prepared daily before administration using $^{57}FeCl_3$ and $^{58}FeCl_3$ solutions as given in the section 'Production of hybrids'. These solutions were prepared beforehand by dissolving ^{57}Fe and ^{58}Fe in excess concentrated HCl and by adding H_2O_2 to oxidize Fe(II) to Fe(III). This solution was then evaporated to near dryness, re-dissolved in 0.01 M HCl, and diluted with water to a final concentration of 0.1 M $FeCl_3$. On the other hand, ^{54}Fe was dissolved in 1.5 M H_2SO_4 under argon atmosphere, diluted with water to get a final concentration of 7.1 mM $FeSO_4$ and kept under argon atmosphere until use. Iron in form of ^{57}Fe–FibBLG, ^{58}Fe-Nano and $^{54}FeSO_4$ was gavaged to a final content of 200 μg iron.

Sensory performance

Colour change. Colour change measurements were performed by adding the different iron sources to 100 ml of either chocolate milk, banana milk (103 g banana mixed with 297 g whole milk—3.5% fat, homogenized UHT), raspberry drink yogurt, cereal-based infant porridge (Hipp) and apple–banana-based infant puree (Hero) (all foods were purchased at the Migros supermarket chain, Zurich, Switzerland). Two different fortification levels of 2.5 and 5 mg iron per 100 g food were used. Both levels are higher than the typically applied (2 mg per 100 g) to identify any possible colour changes[51]. Colour change was measured in duplicate after stirring the powder for 120 min at 350 r.p.m. The matrix was transferred to the cuvette (5.5 cm inner diameter) and placed on the light projection tube of a spectral photometer (Chroma-Meter CR-310, Minolta Schweiz AG) and measured in triplicate after rotating the dish each time by 120°. Absolute colour change (ΔE^*_{ab}) was measured using the Hunter Lab colour system and calculated as follows:

$$\Delta E^*_{ab} = \sqrt{(\Delta L^*)^2 + (\Delta a^*)^2 + (\Delta b^*)^2}$$

where ΔL^* (lightness), Δa^* (chromaticity coordinate) and Δb^* (chromaticity coordinate) correspond to the difference between the sample (with added compound) and the not fortified matrix. $FeSO_4$ and ferric pyrophosphate (FePP, 20% Fe, food quality micronized powder, P. Lohmann GmbH, Germany) were used as positive and negative controls, respectively.

Turbidity measurement. Local Thai fish sauce (Tiparos fish sauce, Thailand; fish extract 65%, water, table salt, sugar) was fortified with 25 mg Fe per 100 ml fish sauce according to ref. 52. Approximately 20 ml of each fortified fish sauce batch were stored in clear glass bottles at room temperature in a laboratory hood for one month. There was no special setting for light exposure. The samples were exposed to indirect sunlight, normal light and to dark, depending on the time of the day, mimicking the conditions of a household.

Turbidity (T) after Fe fortification with liquid form Fe–FibBLG was compared with $FeSO_4$, Fe pyrophosphate. Turbidity was measured using the UV–vis (SPECORD 200 Plus, Analytikjena AG) spectrometer by determining the intensity of stray light passing through the liquid sample. Formazin solution was prepared according to the applicant manual using non-diluted fish sauce as a reference. Once the standard curve for adjusted fish sauce using the Formazin solution was created, the absorbance of each sample was measured with UV–Vis after the samples were carefully well shaken. The turbidity (FNU) values of the samples were extrapolated from the standard curve, as absorbance was plotted against FNU units and evaluated relative to the Formazin stock solution. Finally, the absolute FNU values measured for unfortified fish sauce (stored for one month) were subtracted from all FNU values of fortified fish sauce and ΔT was obtained.

Data availability. All relevant data are included in the manuscript and supporting information. These are also available from the authors upon request.

References

33. Jung, J. M. & Mezzenga, R. Liquid crystalline phase behavior of protein fibers in water: experiments versus theory. *Langmuir* **26,** 504–514 (2010).
34. Li, X., Elliott, D. W. & Zhang, W. Zero-valent iron nanoparticles for abatement of environmental pollutants: materials and engineering aspects. *Crit. Rev. Solid State Mater. Sci.* **31,** 111–122 (2006).
35. Amar-Yuli, I. *et al.* Templating effects of lyotropic liquid crystals in the encapsulation of amyloid fibrils and their stimuli-responsive magnetic behavior. *Soft Matter* **7,** 3348–3357 (2011).
36. Hoffmann, M. A. M. & van Mil, P. J. J. M. Heat-induced aggregation of β-lactoglobulin: role of the free thiol group and disulfide bonds. *J. Agric. Food Chem.* **45,** 2942–2948 (1997).
37. Gao, G.-Q. & Xu, A.-W. A new fluorescent probe for monitoring amyloid fibrillation with high sensitivity and reliability. *RSC Adv.* **3,** 21092–21098 (2013).
38. Lara, C., Adamcik, J., Jordens, S. & Mezzenga, R. General self-assembly mechanism converting hydrolyzed globular proteins into giant multistranded amyloid ribbons. *Biomacromolecules* **12,** 1868–1875 (2011).
39. Bolisetty, S., Vallooran, J. J., Adamcik, J. & Mezzenga, R. Magnetic-responsive hybrids of Fe_3O_4 nanoparticles with β-lactoglobulin amyloid fibrils and nanoclusters. *ACS Nano* **7,** 6146–6155 (2013).
40. Sears, V. F. Neutron scattering lengths and cross sections. *Neutron News* **3,** 26–37 (1992).
41. Breßler, I., Kohlbrecher, J. & Thünemann, A. F. SASfit: a tool for small-angle scattering data analysis using a library of analytical expressions. *J. Appl. Crystallogr.* **48,** 1587–1598 (2015).
42. Reeves, P. G. AIN-93 purified diets for laboratory rodents: final report of the American Institute of Nutrition ad hoc writing committee on the reformulation of the AIN-76A rodent diet. *J. Nutr.* **123,** 1939–1951 (1993).

43. Rahman, I., Kode, A. & Biswas, S. K. Assay for quantitative determination of glutathione and glutathione disulfide levels using enzymatic recycling method. *Nat. Protoc.* **1,** 3159–3165 (2007).
44. Toblli, J. E., Cao, G., Olivieri, L. & Angerosa, M. Comparative study of gastrointestinal tract and liver toxicity of ferrous sulfate, iron amino chelate and iron polymaltose complex in normal rats. *Pharmacology* **82,** 127–137 (2008).
45. Brown, B. E. *et al.* Red cell, plasma, and blood volume in healthy women measured by radiochromium cell-labeling and hematocrit. *J. Clin. Invest.* **41,** 2182–2190 (1962).
46. Lee, H. B. & Blaufox, M. D. Blood volume in the rat. *J. Nucl. Med.* **25,** 72–76 (1985).
47. Walczyk, T. Iron isotope ratio measurements by negative thermal ionisation mass spectrometry using FeF_4^- molecular ions. *Int. J. Mass Spectrom. Ion Process.* **161,** 217–227 (1997).
48. Walczyk, T., Davidsson, L., Zavaleta, N. & Hurrell, R. F. Stable isotope labels as a tool to determine the iron absorption by Peruvian school children from a breakfast meal. *Fresenius J. Anal. Chem.* **359,** 1588–1590 (1997).
49. Lopes, T. J. S. *et al.* Systems analysis of iron metabolism: the network of iron pools and fluxes. *BMC Syst. Biol.* **4,** 1–18 (2010).
50. Hotz, K., Krayenbuehl, P. & Walczyk, T. Mobilization of storage iron is reflected in the iron isotopic composition of blood in humans. *JBIC J. Biol. Inorg. Chem.* **17,** 301–309 (2012).
51. Hurrell, R. F. Ferrous fumarate fortification of a chocolate drink powder. *Br. J. Nutr.* **65,** 271–283 (1991).
52. Fidler, M. C., Krzystek, A., Walczyk, T. & Hurrell, R. F. Photostability of sodium iron ethylenediaminetetraacetic acid (NaFeEDTA) in stored fish sauce and soy sauce. *J. Food Sci.* **69,** S380–S383 (2004).